J Solid State Eletrochem (2004) 8: 532–537
DOI 10.1007/s10008-003-0474-9

ORIGINAL PAPER

Renato Canha Ambrosio · Edson A. Ticianelli

Platinum alloying effects on the behavior of a metal hydride electrode

Received: 25 August 2003 / Accepted: 2 November 2003 / Published online: 9 January 2004

Abstract This is a study of the alloy structure, cycling life, and reaction kinetics of $LaNi_{4.7-x}Sn_{0.3}Pt_x$ ($x = 0$ and 0.1) metal hydride electrodes, using X-ray diffraction, X-ray absorption spectroscopy, electrochemical charge/discharge cycling, and electrochemical impedance spectroscopy. It is seen that the presence of platinum in the alloy causes an increase of the cycle life and a decrease in the hydrogen equilibrium pressure, activation time, charge storage capacity, and the rate of capacity decay during multicycling. XANES results are consistent with a decrease in the Ni oxidation in the Pt-containing alloy after the electrode cycling, indicating a protection introduced by Pt against Ni oxidation. It was also found that the catalytic activity of charge/discharge is improved with Pt alloying, a factor exclusively related to an increase of the active area due to higher alloy pulverization.

Keywords Cycle life stability · Hydrogen oxidation reaction · Hydrogen storage alloys · Platinum · X-ray absorption spectroscopy

Introduction

Although the $LaNi_5$ alloy presents high hydrogen absorption/desorption capacity, easy electrochemical activation, and fast charge/discharge reaction kinetics, the charge storage capacity of this alloy declines rapidly during the first charge/discharge cycles due to the oxidizing decomposition of the alloy, forming $La(OH)_3$ [1]. The cycle life of this material is dramatically improved if a small fraction of the Ni is replaced by Sn [2, 3, 4]. Addition of Co, partially replacing the Ni, is also very effective to further enhance the cycle life of the $LaNi_{4.7}Sn_{0.3}$ alloy [3]. The effects of various other ternary substitutions of Ni in $LaNi_5$ have been also studied, and the results show that cycle life improves with ternary substituents in the order $Mn < Ni < Cu < Cr < Al < Co$ [2].

Markin et al. [5] described the reduction of $LaNi_5$ degradation over the electrochemical cycling after painting the electrode surface with Pt-black. Also, the Pt-black coating was shown to be effective to catalyze the recombination of dissolved oxygen with hydrogen. Even though Pt has proven to be a very effective catalyst for the hydrogen oxidation/evolution reaction, so far no work had been devoted to study the Pt alloying effects on the physical and electrochemical properties of metal hydride materials. Improvements in the charge/discharge reaction kinetics are always required for many metal hydride battery applications, particularly for electric automobiles, laptops, and cellular phones.

In this paper, a systematic study of the effects of Pt alloying on the physical and electrochemical properties of a AB_5 metal hydride alloy is presented. X-ray absorption spectroscopy measurements, conducted at the Ni K-edge, were carried out to characterize the effects of Pt and the alloy cycling on the electronic properties of Ni atoms. Kinetic studies were performed by electrochemical charge/discharge cycling and impedance spectroscopy. To the best of our knowledge, this study corresponds to the first contribution for the characterization of the electronics and cycling properties and the reaction kinetics of a Pt-alloyed AB_5 hydrogen storage material.

Experimental

The metal hydride alloys were prepared from high-purity metals by the arc melting technique under an inert gas atmosphere. Ingots were re-melted four times and then annealed for 72 h in vacuum at 950 °C to ensure good homogeneity. Energy dispersive X-ray analyses (EDX, 100 times magnification) made at several spots confirmed, within experimental error, the nominal composition of

R. C. Ambrosio · E. A. Ticianelli (✉)
Instituto de Química de São Carlos, USP,
Av. do Trabalhador Sãocarlense 400, Caixa Postal 780,
CEP 13560-970 São Carlos, SP, Brazil
E-mail: edsont@iqsc.usp.br

the alloy. Alloy powder with a mean particle size less than 30 μm was obtained by crushing using a mechanical method. X-ray diffraction (XRD) patterns confirmed the hexagonal $CaCu_5$-type structure of the alloy.

Electrodes were prepared by pressing a mixture composed of 0.050 g of the active powder, 0.050 g of carbon black (Vulcan XC-72), and 33 wt% polytetrafluoroethylene (PTFE) binder, on both sides of a nickel screen with a geometric area of 2 cm^2. Electrochemical measurements were done in a three-electrode cell in 6 mol L^{-1} KOH, with a Pt mesh counter electrode and a Hg/HgO-KOH 6 mol L^{-1} reference electrode.

Cycle-life tests were carried out by charging the electrode with a cathodic current of 10 mA (200 mA per gram of the alloy) and discharging with an anodic current of the same magnitude to a cutoff cell potential of −700 mV vs. Hg/HgO. Kinetic impedance measurements were made when the electrode charging capacity had reached the maximum, with the electrodes maintained at open-circuit potential, for several states of charge and temperatures. The electrochemical impedance spectra (EIS) were recorded in the frequency range of 10 kHz to 1 mHz, with an a.c. amplitude of 5 mV. For measurements of the hydrogen equilibrium pressure as a function of the state of charge, the activated electrode was fully charged and maintained at open circuit until the potential reached equilibrium (variation of less than 0.1 mV min^{-1}). Then, the electrodes were partially discharged and the equilibrium potential measured again. This procedure was repeated until the electrode was fully discharged. The partial hydrogen pressures were calculated from the equilibrium potential $\left(E_{MH}^{eq}\right)$ using the Nernst equation [6].

X-ray absorption spectroscopic (XAS) measurements were conducted at the XAS beam line at the LNLS, National Synchrotron Light Source, Brazil. In this line, the radiation is monochromatized using a Si(111) single crystal. The data acquisition set-up is composed of three ionization chambers (incident, transmittance, and reference detectors). The reference channel was primarily used for internal calibration of the edge position, using pure metal foil for Ni. Analyses were carried out in the transmittance mode at the Ni K-edge.

Samples for the XAS measurements were prepared by pressing a mixture of 20 mg of the alloy powder with 50 mg of Teflonized carbon, in a form of a disc with 1 cm^2 geometric area. Data analysis was conducted using the WinXAS software [7]. XANES (X-ray absorption near edge structure) spectra were first corrected for the background absorption by fitting the pre-edge data (from −60 to −20 eV below the edge) to a linear formula, followed by extrapolation and subtraction from the data over the energy range of interest. Finally, the spectra were normalized, taking as reference a second polynomial function obtained by fitting the data throughout the EXAFS (extended X-ray absorption fine structure) oscillations, starting 50 eV above the edge. Next, the spectra were calibrated for the edge position, at the inflection point of the edge jump of the data from the reference channel, using the second derivative method.

Results and discussion

X-ray diffractometry was used to characterize the microstructure and measure the lattice parameters of the metal hydride alloys with and without Pt. Figure 1 shows the diffraction patterns for the $LaNi_{4.7}Sn_{0.3}$ and $LaNi_{4.6}Sn_{0.3}Pt_{0.1}$ alloys. The results confirmed that the alloys present hexagonal $CaCu_5$-type structures, with no evidence for formation of any segregated phase. The diffraction peaks shift to smaller angles due to the presence of platinum in the alloy, indicating an increase of the lattice parameters or of the unit cell volume.

Figure 2a shows the charge/discharge potential versus time profiles obtained for both electrodes at the 10th

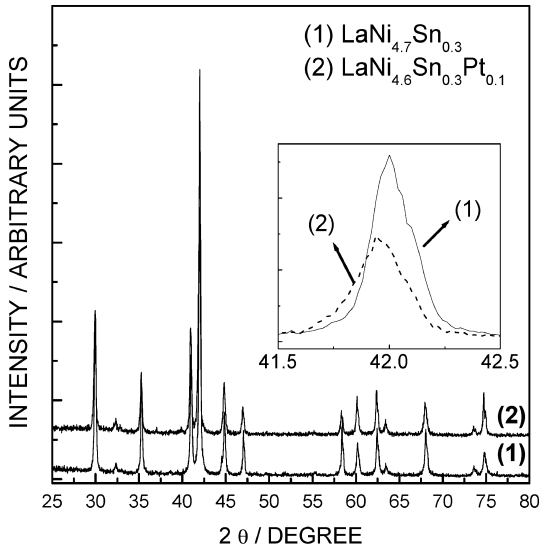

Fig. 1 X-ray diffraction patterns for $LaNi_{4.7}Sn_{0.3}$ (*1*) and $LaNi_{4.6}Sn_{0.3}Pt_{0.1}$ (*2*) alloy powders. The *inset* shows the diffraction peak shifting to smaller angles with the introduction of Pt

cycle. In each case, well-defined charge/discharge plateaus are observed. Figure 2b shows the evolution of the plateau potentials as a function of cycle number for both electrodes. In Fig. 2b, it is seen that the $LaNi_{4.6}Sn_{0.3}Pt_{0.1}$ electrode presents smaller discharge overpotentials compared to the $LaNi_{4.7}Sn_{0.3}$ electrode for all the measured cycles. This is a consequence of the fact that the exchange current density for the hydrogen oxidation reaction (HOR) on the Pt-alloyed MH electrode is higher than that of the $LaNi_{4.7}Sn_{0.3}$ alloy, as will be shown from the EIS results. A lower discharge potential leads to a higher specific power for the battery. On the other hand, there is a decrease in the total discharge time for the Pt-containing alloy. In Fig. 2b it is also seen that the charging overpotential decreases during the first 15 cycles, until reaching a constant value.

Plots of the discharge capacity are presented in Fig. 3 for $LaNi_{4.7-x}Sn_{0.3}Pt_x$. It is seen that at the eighth cycle the $LaNi_{4.7}Sn_{0.3}$ electrode reaches the maximum discharge capacity, while the activation time decreases almost to zero for the Pt-alloyed MH electrode. It is well accepted that this so-called activation process is a consequence of the reduction of natural oxide covering the powder particles and/or of the decrease of the particle size caused by a stress cracking process due to the lattice expansion/contraction occurring upon hydride formation/decomposition. In the present cases, the smaller activation time observed for the Pt-containing alloy can be associated with the smaller particle size of this alloy, as evidenced by the less sharp XRD peaks in Fig. 1. A decrease in the normalized hydrogen storage capacity is observed for the alloy containing Pt and this can be explained by taking into account that substitution of Ni by Pt involves the replacement of a low atomic weight atom by a high atomic weight atom, without changing the number of interstitial sites. Another possibility is that the

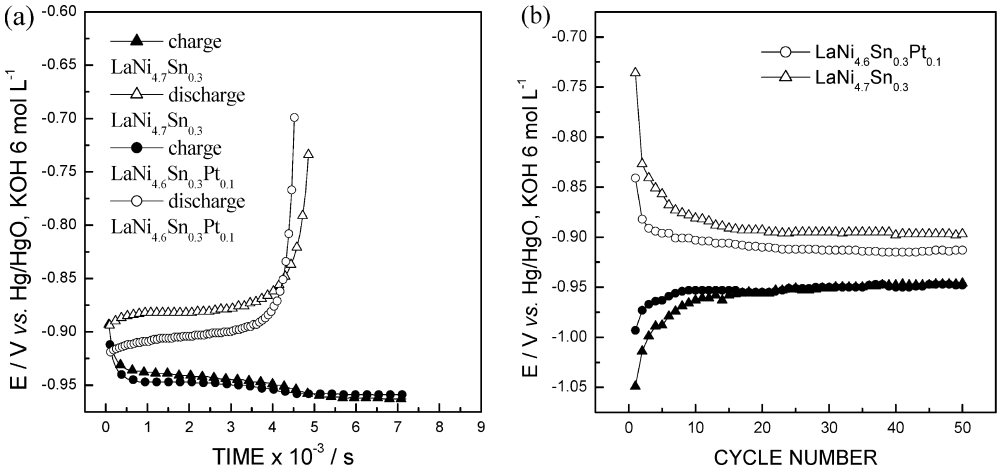

Fig. 2 (**a**) Charge and discharge profiles for the 10th cycle for the $LaNi_{4.7}Sn_{0.3}$ and $LaNi_{4.6}Sn_{0.3}Pt_{0.1}$ alloy electrodes. Discharge current = 200 mA g^{-1}. (**b**) Variation of the discharge (midpoint value) plateau potentials and the potentials at the end of charge as a function of the cycle number

decrease in the hydrogen storage capacity of the Pt-containing alloy is caused by changes in the electronic structure of the alloy due to the platinum alloying. Comparing the discharge capacity versus cycle number profiles, it is seen that the Pt-containing electrode presents a smaller capacity decay, consistent with the higher unit cell volume of this material, which reduces the pulverization and thus the material oxidation by the alkaline electrolyte throughout the charge/discharge cycles.

Figure 4 presents representative XANES results in the transmission mode at the Ni K-edge for uncycled and cycled (100 cycles) $LaNi_{4.7}Sn_{0.3}$ and $LaNi_{4.6}Sn_{0.3}Pt_{0.1}$ alloys. Absorptions at the Ni K-edge are due to excitations of 1s electrons to electronic states above the Fermi level [8, 9]. Because of the selection rule at the K-edge, only transitions into empty p states are dipole allowed. For Ni, theoretical calculations show that there is mixing of p and d states and, as a result, transitions into the empty p-like part of these mixed p–d states can occur [8, 10]. This is responsible for the appearance of the pre-edge peak at about 3.0 eV (Fig. 4). In a series of metal hydride alloys in which the unit cell symmetry is maintained, the intensity of this pre-edge absorption feature may be taken as a measure of the occupancy of the p-like electronic energy states in the metal d-band [8, 9].

No apparent effect is introduced in the pre-edge region by replacement of Ni by Pt for the uncycled alloys, indicating that there were no significant changes in the Ni p–d density of states due to the presence of Pt. On the other hand, for the cycled alloys it is seen that both the $LaNi_{4.7}Sn_{0.3}$ and $LaNi_{4.6}Sn_{0.3}Pt_{0.1}$ alloys show some oxidation of the Ni atoms after 100 cycles, as concluded from the increase of the intensity of the edge-hump around 20 eV. This seems to be one of the causes of performance degradation after alloy multicycling. Compared to the Pt-containing alloy, a larger decrease in the pre-edge region is seen for the $LaNi_{4.7}Sn_{0.3}$ alloy, consistent with a higher Ni oxidation [2]. Thus, this result indicates some protection against the oxidation of Ni atoms introduced by Pt, implying a higher stability of the Pt-containing material.

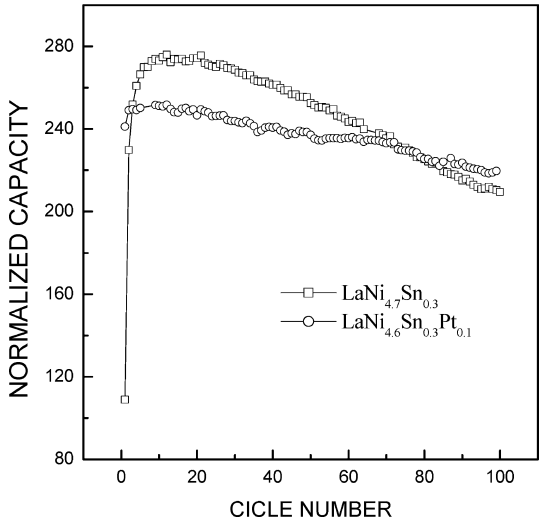

Fig. 3 Discharge capacity versus cycle number. Charge/discharge current, 200 mA g^{-1}; charging time, 2 h; discharge cut-off potential, −0.7 V vs. Hg/HgO

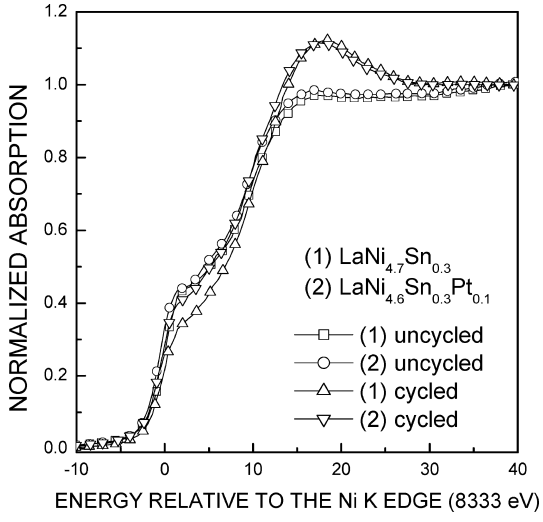

Fig. 4 XANES spectra in the transmission mode at Ni K-edge for uncycled and cycled (100 cycles) $LaNi_{4.7}Sn_{0.3}$ and $LaNi_{4.6}Sn_{0.3}Pt_{0.1}$ alloys

Figure 5 shows the electrochemically measured hydrogen equilibrium pressure plotted as a function of the state of charge of the electrodes. It is clear that for states of charge smaller than 80%, the hydrogen equilibrium pressure reaches a plateau and that the magnitude of the plateau is somewhat smaller for the sample containing Pt. A diminution of pressure may be related to the formation of a stronger M–H bond and/or to a smaller compression (chemical potential or scaping tendency) of the H atoms inside the unit cell. Previous results have shown that formation of hydride bonds are predominantly made through the Ni atoms [9, 10, 11]. XANES results for uncycled samples (Fig. 4) indicated no significant change in the energy of the Fermi level or in the occupancy of the p-like electronic states of the Ni atoms due to the presence of Pt. This implies that the Ni–H bond should present a similar strength in both samples. Thus, the slight decrease of the plateau pressure for the $LaNi_{4.6}Sn_{0.3}Pt_{0.1}$ material may be explained by the increase of the unit cell volume introduced by platinum, as seen from the XRD results. This would diminish the compression of the H atoms, as already proposed for other metal hydride alloys [12].

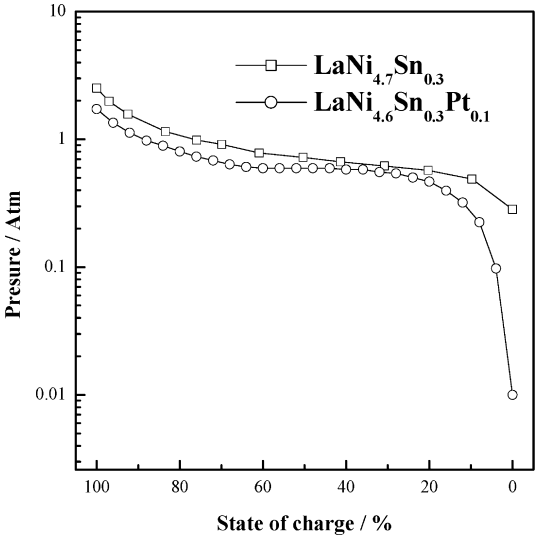

Fig. 5 Hydrogen equilibrium pressure versus state of charge of the electrodes

Figure 6 shows the electrochemical impedance spectra for the activated $LaNi_{4.7}Sn_{0.3}$ and $LaNi_{4.6}Sn_{0.3}Pt_{0.1}$ alloys, obtained at several temperatures for fully charged electrodes. Figure 7 shows the corresponding results for the same alloys in the charged and discharged states. In all these plots, the impedances in the real axes were subtracted by the high-frequency impedance (mainly associated with the electrolyte resistance). Firstly it should be noted that these impedance responses are qualitatively similar to the results presented for other metal hydride alloys [2, 3]. The results show only one important arc with a magnitude and characteristic frequency dependent on the temperature, electrode composition, and state of charge. Previous works have shown that this feature is related to the kinetics of the charge transfer step [2, 3] of the hydriding/dehydriding processes, that is:

$$S - H_{abs}(\text{bulk}) \rightleftharpoons S - H_{ads}(\text{surface}) \qquad (\text{diffusion}) \tag{1}$$

$$S - H_{ads} + OH^- \rightleftharpoons H_2O + S + e^- \qquad (\text{charge transfer}) \tag{2}$$

According to this, the exchange current density (i_0) for the charge transfer step is evaluated from the radius of this arc (R_{ct}), using the Butler–Volmer equation in the limit of low overpotentials, that is:

$$i_0 = \frac{RT}{nF}\left(\frac{1}{R_{ct}}\right) \tag{3}$$

where F is Faraday's constant, R is the gas constant, and T is the temperature. Values of i_0 of 96 mA g^{-1} and 283 mA g^{-1} resulted for the $LaNi_{4.7}Sn_{0.3}$ and $LaNi_{4.6}Sn_{0.3}Pt_{0.1}$ metal hydride electrodes at 25 °C and 100% state of charge.

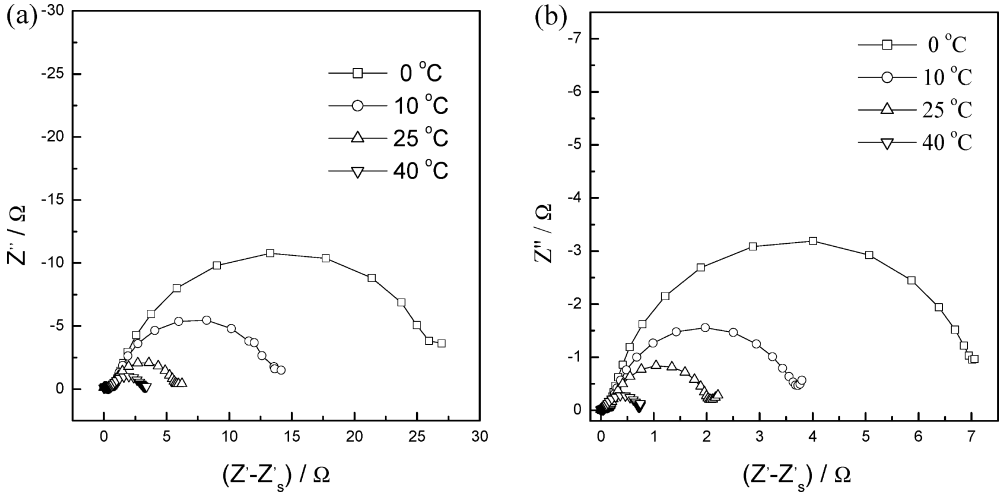

Fig. 6 Nyquist plots at several temperatures for (**a**) $LaNi_{4.7}Sn_{0.3}$ (10th cycle) and (**b**) $LaNi_{4.6}Sn_{0.3}Pt_{0.1}$ (3rd cycle) fully charged electrodes

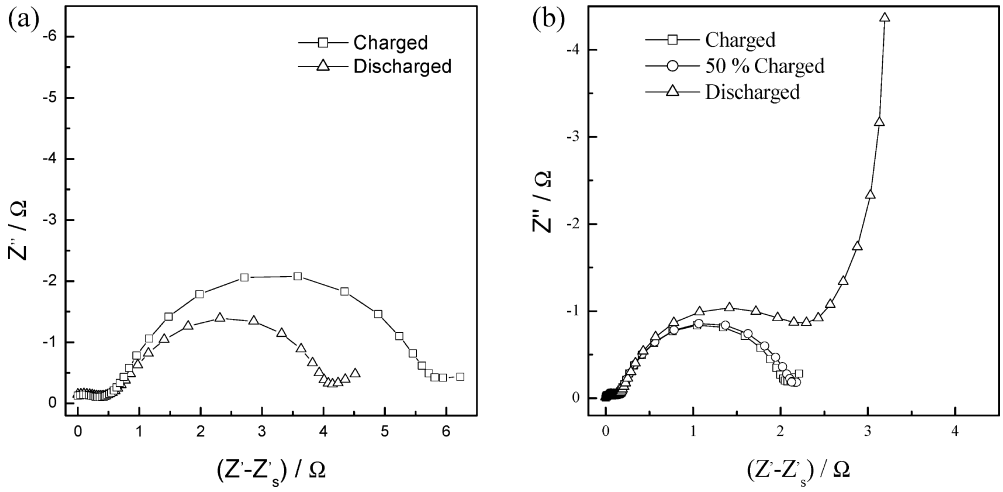

Fig. 7 Nyquist plots for (**a**) $LaNi_{4.7}Sn_{0.3}$ and (**b**) $LaNi_{4.6}Sn_{0.3}Pt_{0.1}$ electrodes at several sites of charge at 298 K

For the $LaNi_{4.7}Sn_{0.3}$ electrode it is seen that the magnitude of the impedance arc is smaller for the discharged electrode (Fig. 7a). This means that for the $LaNi_{4.7}Sn_{0.3}$ alloy the discharge of the electrode results in an increase of the exchange current density of the HOR (see Eq. 3), as also observed for other metal hydride alloys [2, 3]. In aqueous alkaline electrolysis it is well known that the kinetics of hydrogen evolution on nickel cathodes decreases with time. This has been attributed to the hydriding of the nickel [2]. A similar mechanism may be occurring here on the metallic surface species responsible for the catalytic processes. For the Pt-containing alloy, the magnitude of the impedance arcs are similar for all states of charge, including the uncharged electrode, meaning that in this case the catalytic activity for the HOR is essentially independent of the hydride content in the alloy. This behavior is consistent with the presence of some Pt atoms on the alloy surface, which must participate in the catalysis of HOR with constant activity, independent of the state of charge.

Measurements of i_0 were also conducted at several temperatures in order to obtain the activation energy of the hydrogen oxidation step (reaction 2). Figure 8 presents the plots of $\ln i_0$ vs. $1/T$ for both electrodes. It is observed that the slopes of the graphs are similar, meaning that, within experimental error, the activation energy is not affected by the Pt presence (here $E^{\neq} \approx 40$ kJ mol^{-1}). This is a somewhat surprising result, since it would be expected that the presence of Pt should lead to an increase in the reaction kinetics resulting from a decrease of the activation energy for the HOR. The similarities of the activation energies can be explained by taking into account that, for the present stoichiometric compositions, only a small amount of Pt is located on the alloy particle surface, thus not affecting significantly the catalytic properties of the HOR. So, the higher exchange current density observed for this material (Fig. 8) must be predominantly a consequence of the higher surface area (smaller average particle size) of this alloy powder, as seen from the XRD measurements.

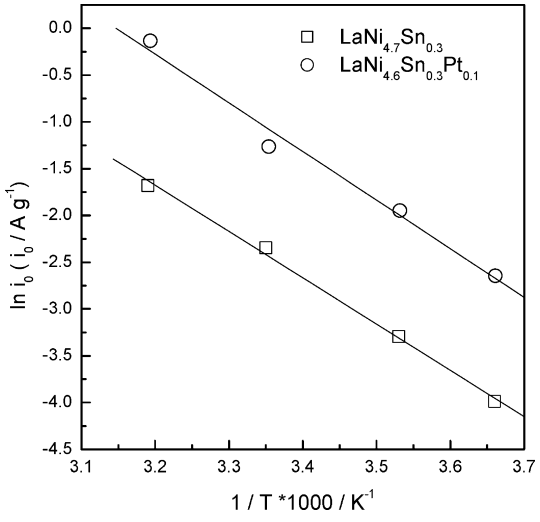

Fig. 8 Arrhenius plots ($\ln i_0$ vs. $1/T$) for the $LaNi_{4.7}Sn_{0.3}$ and $LaNi_{4.6}Sn_{0.3}Pt_{0.1}$ electrodes

Reaction 2 shows that a crucial step for the hydrogen oxidation electrocatalysis is the breaking of the Ni–H bond, which should be formed from hybridization of d electrons from Ni and the 1s electron from the hydrogen atom [9, 10]. A more filled d band will imply that the hybridization will involve less bonding electrons, leading to the formation of weaker Ni–H bonds [11]. In the present cases, the XANES results in Fig. 2 do not indicate any difference in the electronic structure of the Ni atoms in the presence or absence of platinum. This fact can also explain the similarity of the values of the activation energy for the alloys studied in this work.

Conclusions

Electrochemical experiments were conducted on metal hydride electrodes to analyze the effects of Pt on the properties of a AB_5-type alloy. It is seen that the presence of platinum causes an increase of the cycle life and

a decrease in the hydrogen equilibrium pressure, the activation time, the charge storage capacity, and the rate of capacity decay. XANES results are consistent with a decrease in Ni oxidation for the Pt-containing alloy after electrode cycling, indicating a protection introduced by Pt against Ni oxidation.

An expansion of the unit cell volume occurs due to the presence of Pt. This fact, combined with the observation that the maximum charge storage capacity is smaller for this material, implies a smaller compression of the hydrogen atoms inside the M–H particle, resulting in a reduction of the hydrogen equilibrium pressure. This may also lead to a decrease in the stress cracking process, thus raising the stability of the material.

The main impedance features of the metal hydride electrodes were related to the charge transfer step of the hydriding/dehydriding processes. It was found that the catalytic activity of charge/discharge is improved with Pt alloying, a factor exclusively related to a higher active area (smaller particle size). XANES experiments indicated a negligible effect of Pt on the electronic properties of Ni atoms, implying the formation of similar strength metal–hydrogen bonds. This explains the similar values for the activation energy of the charge transfer step in the hydriding/dehydriding reaction.

Acknowledgements The authors wish to thank Fundação de Amparo à Pesquisa do Estado de São Paulo (FAPESP) and the LNLS, National Synchrotron Light Laboratory, Brazil for financial and technical support.

References

1. Jung JH, Lee HH, Kim DM, Jang KJ, Lee JY (1998) J Alloys Compd 266:266
2. Ticianelli EA, Mukerjee S, McBreen J, Adzic GD, Johnson JR, Reilly JJ (1999) J Electrochem Soc 146:3582
3. Ambrosio RC, Ticianelli EA (2002) J Power Sources 110:73
4. Ratnakumar BV, Witham C, Bowman RC, Hightower A, Fultz B (1996) J Electrochem Soc 143:2578
5. Markin TL, Dell RM (1981) J Electroanal Chem 118:217
6. Notten PHL, Latroche M, Guégan AP (1999) J Electrochem Soc 146:3181
7. Ressler T (1997) J Phys IV C2:269
8. Lengeler B, Zeller R (1984) J Less-Common Met 103:337
9. Gupta M (1987) J Less-Common Met 130:219
10. Tryk DA, Bae IT, Hu Y, Kim S, Antonio MR, Scherson DA (1995) J Electrochem Soc 142:824
11. Jaksic JM, Ristic NM, Krstajic NV, Jaksic MM (1998) Int J Hydrogen Energy 23:1121
12. Kumar MPS, Zhang W, Petrov K, Rostami AA, Srinivasan S, Adzic GD, Johnson JR, Reilly JJ, Lim HS (1995) J Electrochem Soc 142:3424